Title: Inhibitory interneurons show early dysfunction in a SOD1 mouse model of ALS

Abbreviated Title: Dysfunction of inhibitory interneurons in ALS

C. F. CAVARSAN[1,2], P. R. STEELE[1,2,3], L. M. McCANE[3], K. J. LaPRE[1,2], A. C. PURITZ[4], N. KATENKA[5], AND K. A. QUINLAN[1,2,4]

1 George and Anne Ryan Institute for Neuroscience, University of Rhode Island, Kingston, RI, 02881 USA
2 Department of Biomedical and Pharmaceutical Sciences, College of Pharmacy, University of Rhode Island, Kingston, RI, 02881 USA
3 Interdisciplinary Neuroscience Program, University of Rhode Island, Kingston, RI, 02881 USA
4 Department of Physiology, Northwestern University Feinberg School of Medicine, Chicago, IL, 60611 USA
5 Department of Computer Science and Statistics, University of Rhode Island, Kingston, RI, 02881 USA

Corresponding Author:
Katharina A. Quinlan
kaquinlan@uri.edu
George and Anne Ryan Institute for Neuroscience
University of Rhode Island
130 Flagg Rd
Kingston RI 02881

Number of pages: 35
Number of figures: 8
Number of tables: 5
Number of words in abstract: 238
Number of words in introduction: 621
Number of words in discussion: 1820

Abstract: Few studies in amyotrophic lateral sclerosis (ALS) focus on the inhibitory interneurons synapsing onto motoneurons (MNs). However, inhibitory interneurons could contribute to dysfunction, particularly if altered before MN neuropathology and establishing a long-term imbalance of inhibition / excitation. We directly assessed excitability and morphology of glycinergic (GlyT2) interneurons located throughout the ventral horn in the lumbar enlargement from SOD1^{G93A}GlyT2eGFP (SOD1) and wildtype GlyT2eGFP (WT) mice on postnatal day 6 to 10. Patch clamp revealed dampened excitability in SOD1 interneurons, including depolarized persistent inward currents (PICs), depolarized threshold for firing action potentials, and a shortened afterhyperpolarization (AHP). SOD1 inhibitory interneurons also had smaller soma but increased dendritic volume and surface area. GlyT2 interneurons were then divided into 3 subgroups based on location: interneurons within 100 µm of the ventral white matter where Renshaw cells (RCs) are located, interneurons interspersed with MNs in lamina IX, and interneurons in the intermediate ventral area including laminae VII and VIII. Lamina IX interneurons were the most profoundly affected, including more depolarized PICs, smaller somata and larger dendritic arborization. Interneurons in lamina IX had depolarized PIC onset, smaller somata and longer dendrites. In lamina VII-VIII, interneurons were largely unaffected, mainly showing smaller somata. In summary, inhibitory interneurons show very early region-specific perturbations poised to impact excitatory / inhibitory balance of MNs, modify motor output, and provide early biomarkers of ALS. Therapeutics like riluzole which universally reduce CNS excitability could exacerbate the inhibitory dysfunction described here.

Significance Statement

Spinal inhibitory interneurons could contribute to amyotrophic lateral sclerosis (ALS) pathology as they provide synaptic inhibition to spinal motoneurons (MNs). To investigate their role in the presymptomatic phase, we studied the excitability and morphology of glycinergic interneurons in transgenic mice (SOD1^{G93A}GlyT2eGFP). We found inhibitory interneurons were less excitable and had smaller somas but larger dendrites in SOD1 mice. GlyT2 interneurons were analyzed according to their localization within the ventral spinal cord. Interestingly, the greatest differences were observed in the interneurons located in the ventral most 100 µm. We conclude that inhibitory interneurons show presymptomatic changes that may contribute to excitatory / inhibitory MN dysfunction in ALS.

Key words: inhibition, glycine, Renshaw cells, ALS, spinal cord, patch clamp.

Introduction

Amyotrophic lateral sclerosis (ALS) is a rapidly evolving adult-onset neurological disease characterized by a progressive loss of corticospinal neurons and MNs. There has been considerable debate in the field over the role of hyperexcitability in neurodegenerative processes in ALS. While drug treatment for ALS based on nonspecific reduction of neuronal excitability (with riluzole, for example) (Bellingham 2011), does result in a modest increase in lifespan (Bensimon et al., 1994), similar treatment paradigms have been disappointing clinically. A more nuanced understanding of the excitability of vulnerable neurons could help in creating a more targeted and effective approach for treatment of ALS. For example, if inhibitory pathways are failing in ALS and neuronal excitability is universally reduced with riluzole, this could further exacerbate inhibitory dysfunction by reducing activity not only in vulnerable MNs but also in inhibitory interneurons presynaptic to MNs. Thus it is important to consider all aspects of neuronal excitability, including intrinsic excitability of vulnerable neurons, synaptic drive, and neuromodulation (Gunes et al., 2020). Intrinsic properties of MNs have been well studied but the same is not true for interneurons that are synaptically connected to them. In fact, no studies thus far have directly assessed activity of spinal premotor interneurons in an ALS model.

Despite evidence that ALS patients have disrupted inhibition at spinal levels (Raynor and Shefner, 1994; Shefner and Logigian, 1998; Sangari et al., 2016; Howells et al., 2020; Özyurt et al., 2020), much is still unknown concerning the involvement of inhibitory circuitry in ALS. Morphological alterations in inhibitory circuits have been demonstrated in animal models of ALS. These include degeneration of spinal interneurons, fewer neurons expressing markers of inhibitory neurotransmitters including GlyT2 prior to loss of MNs (Martin et al., 2007; Hossaini et al., 2011), and loss of glycinergic boutons onto MNs prior to symptom onset (Chang and Martin, 2009a). Typically, fast MNs have greater numbers of inhibitory synaptic contacts, but these are largely lost in SOD1 mice beginning when motor unit atrophy is first observed (Pun et al., 2006; Hegedus et al., 2007; Allodi et al., 2021). Recurrent inhibitory circuits mediated by RCs are impaired before symptom onset by both loss of MN collaterals which provide synaptic drive, and complex changes to RC-MN synaptic structures (Casas et al., 2013; Wootz et al., 2013). A few studies have suggested activity is decreased in inhibitory interneurons by indirect measurements. Quantification of synaptic inputs to MNs has shown that frequency of inhibitory postsynaptic potentials in spinal MNs is decreased embryonically in both SOD1 mouse and zebrafish models (McGown et al., 2013; Branchereau et al., 2019) and glycinergic inputs to MNs decay faster in SOD1 MNs (Medelin et al., 2016). On a larger scale, blocking the activity of V1 inhibitory interneurons

105 during *in vivo* treadmill running was recently found to mimic the early locomotor deficits in SOD1 mice
106 (Allodi et al., 2021), suggesting that inhibitory interneurons could be inactive or under-active. However,
107 none of these studies directly examined electrophysiological activity in inhibitory interneurons.
108 We hypothesized that inhibitory spinal interneurons could contribute to the pathogenesis of ALS
109 through a depression of MN inhibition. Decreased activity of inhibitory interneurons could result in
110 synaptically-driven hyperexcitability of MNs and other long-term changes in network function. In this
111 study, we examined electrical and morphological properties of glycinergic interneurons in the spinal
112 cord of SOD^{G93A} GlyT2-eGFP (SOD1) mice compared to GlyT2-eGFP (WT) using whole cell patch clamp
113 and three-dimensional reconstructions. We show here that significant dysfunction is present in SOD1
114 glycinergic interneurons which likely comprise several subclasses of inhibitory interneurons. In general,
115 SOD1 glycinergic interneurons are less excitable and smaller than WT. Impairment in glycinergic
116 interneurons should be explored as both a mechanism of vulnerability of MNs and a potential biomarker
117 of early dysfunction of spinal circuits.
118
119 **Results**
120
121 **Morphology of glycinergic interneurons**
122 Ventrally located glycinergic interneurons in the lumbar enlargement of WT and SOD1 mice postnatal
123 day (P) 6-10 were reconstructed from z-stack images obtained using confocal microscopy. SOD1 GlyT2
124 interneurons were significantly smaller than WT GlyT2 interneurons. Soma volume and surface area
125 were both significantly smaller in SOD1 GlyT2 interneurons found throughout the ventral horn. Typical
126 ventrolateral glycinergic neurons are shown in **Figure 1**. Complete reconstructions of soma morphology
127 were performed on 4138 GlyT2 interneurons (2551 WT and 1587 SOD1 interneurons) from fixed lumbar
128 spinal cords from 18 mice (9 WT and 9 SOD1). See **Table 1** for all morphological parameters. Dendritic
129 morphology was not possible in these images due to the high number of GFP+ neurons and processes
130 but was completed on a smaller subset of neurons that were imaged live after patch clamp
131 electrophysiology with a 2-photon microscope.
132
133

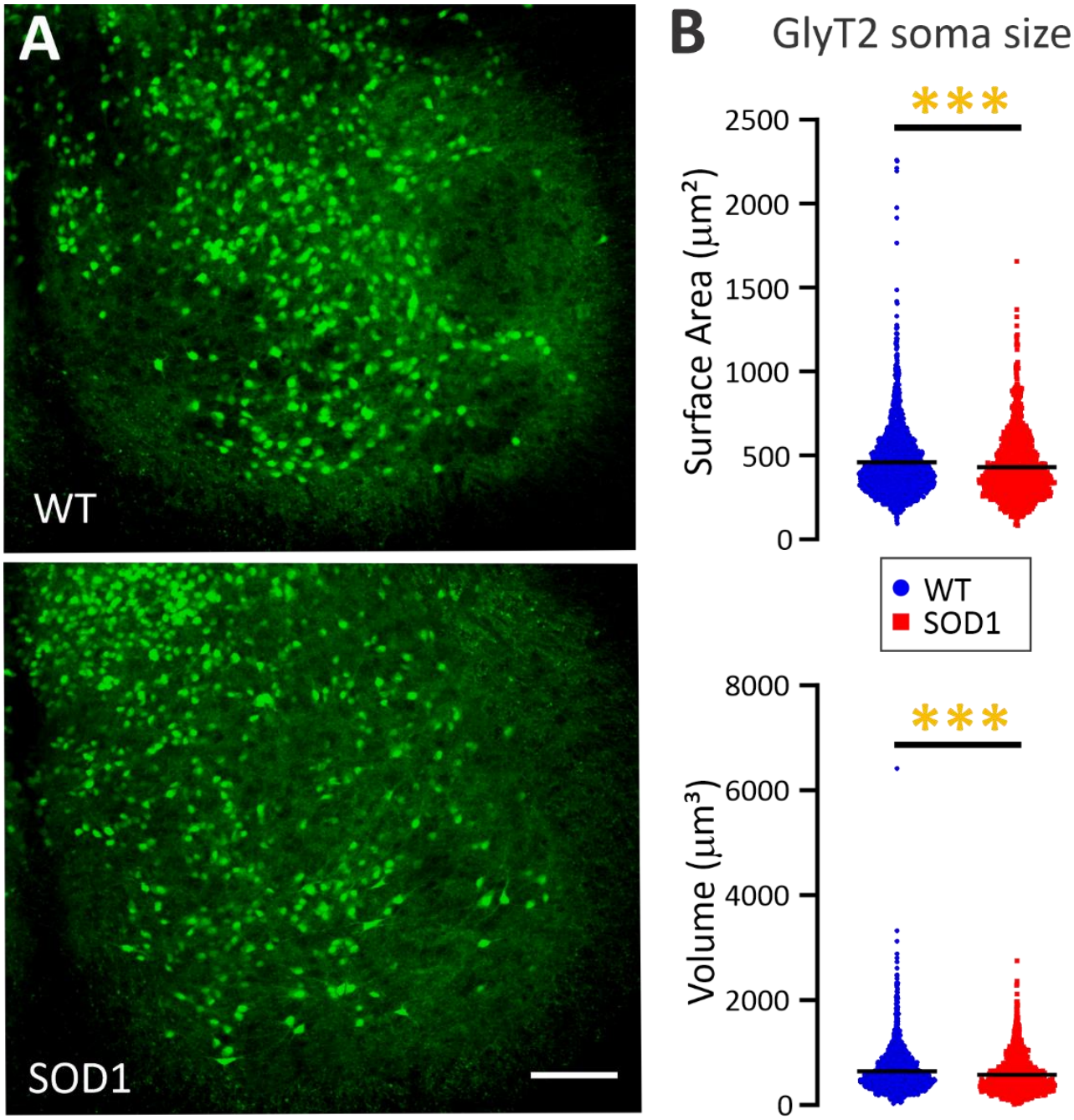

Figure 1: GlyT2 interneurons in the ventral horn from SOD1 mice are smaller than WT. Representative photomicographs of GFP interneurons in **A**. (**B**) Morphological analysis showed SOD1 glycinergic interneurons in ventral horn (N = 1587) were smaller in than WT (N = 2551). Significance denoted with *** indicates $p \leq 0.001$. Scale bar in **A**: 100 μm applies to both images.

135

Table 1: Reconstruction data of GlyT2-GFP+ interneurons in WT and SOD1 animals.

		WT (Mean ± SE)	SOD (Mean ± SE)	*p*
Ventral horn GlyT2-GFP+ Interneurons (somata only)				
		N = 2551	N = 1587	
Soma	Surface Area (µm²)	459.8 (± 4.1)	430.5 (± 4.9) ***	0.000 [K]
	Volume (µm³)	641.1 (± 8.0)	576.5 (± 9.2) ***	0.000 [K]
Patched GlyT2-GFP+ Interneurons				
		N = 34	N =25	
Soma	Surface Area (µm²)	621.1 (± 41.6)	674.6 (± 54.8)	0.728[K]
	Volume (µm³)	1460.2 (± 185.6)	1751.2 (± 222.6)	0.414[K]
Dendrites	Length (µm)	108.5 (± 21.7)	114.4 (± 10.5)	0.152[K]
	Surface Area (µm²)	539.9 (± 87.6)	700.3 (± 53.5) *	0.032[K]
	Volume (µm³)	272.2 (± 48.6)	423.1 (± 40.1) *	0.010[K]

Significance denoted with * indicates $p \leq 0.05$; *** indicates $p < 0.001$.

N is the number of cells included in analysis.

[K] Indicates Kruskal-Wallis Test for nonparametric distributions; all others were ANOVA analysis.

136

137 To study electrophysiological properties of GlyT2 interneurons, 59 glycinergic neurons (34 WT and 25
138 SOD1) were recorded using visually guided patch clamp with Texas Red dye in the electrode as shown in
139 **Figure 2.** The location of patched neurons was distributed throughout the ventral horn as shown in Fig
140 2B. In this smaller sample of neurons, soma sizes of patched SOD1 interneurons were not different (Fig
141 2C). However, dendrites were larger in patched SOD1 GlyT2 interneurons, including greater dendritic
142 surface area and volume (see Table 1 for complete results). Please note that dimensions of these
143 neurons cannot be directly compared to the previous section since these neurons were imaged in living
144 tissue while the previous analysis was performed in fixed tissue, which shrinks.

145

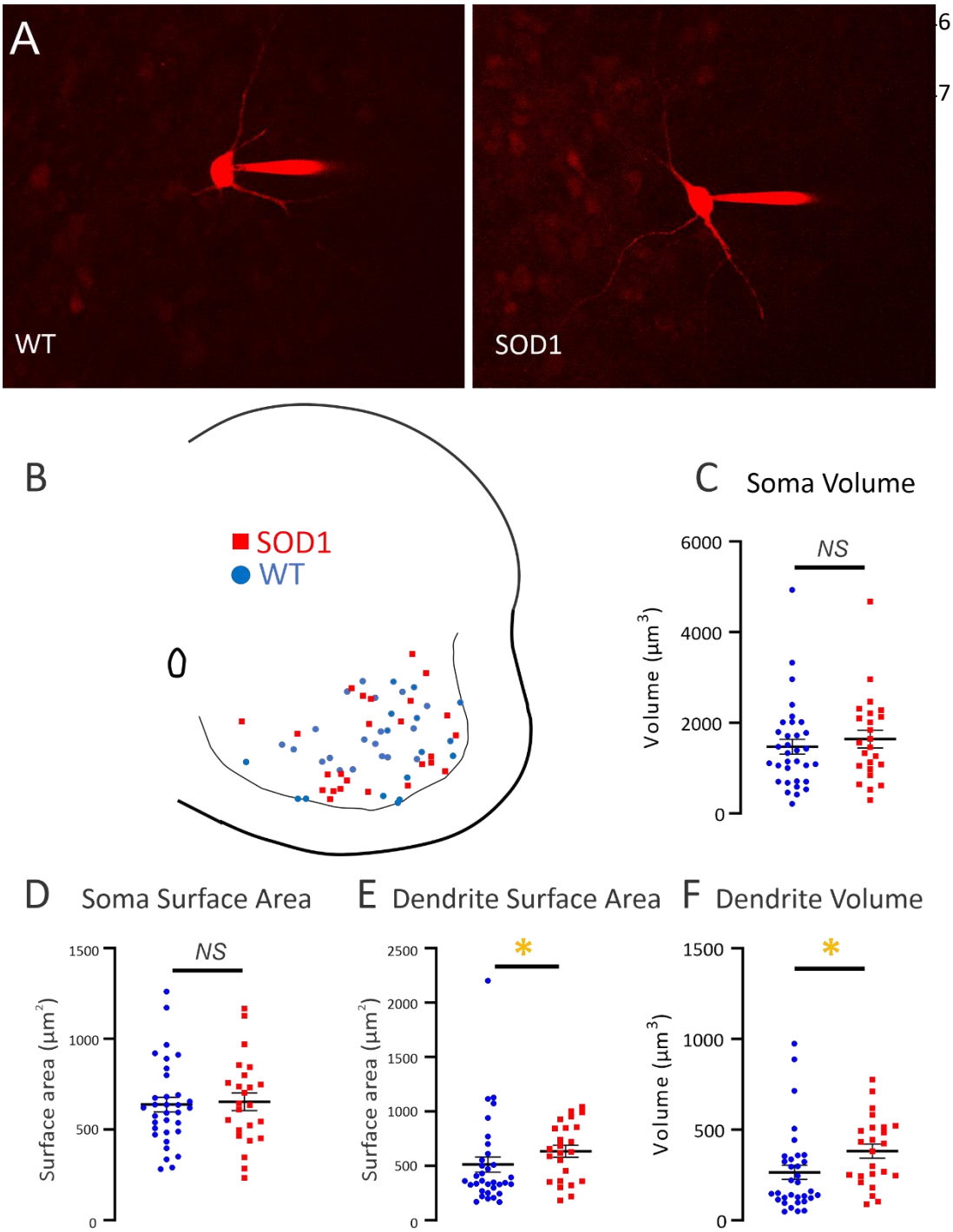

Figure 2 GlyT2 interneurons from WT and SOD1 mice were patched throughout the ventral horn. Images of typical interneurons, filled with Texas Red as they were recorded in **A**, and locations of all patched interneurons in **B** (WT = blue circles, SOD1 = red squares). (**C**) Soma volume and (**D**) soma surface area was unchanged in patched neurons, while dendrite surface area and volume were larger in SOD1 interneurons than in WT. Significance denoted with * indicates $p \leq 0.05$.

Electrophysiology of glycinergic interneurons

Whole cell patch clamp revealed very different intrinsic properties of ventral glycinergic interneurons. Recording was performed on 59 ventral interneurons from throughout the ventral horn in transverse lumbar spinal cord slices from P6-10 mice. SOD1 inhibitory interneurons (n = 25) were found to have diminished intrinsic excitability compared to WT interneurons (n = 34). Measurements of intrinsic excitability included depolarized onset and peak voltage of PICs and depolarized threshold for action potential firing, as shown in **Figure 3**. In voltage clamp, slowly depolarizing voltage ramps were used to measure PICs (typical leak subtracted traces shown in Fig3A). Voltage sensitivity is determined by measuring voltage at PIC onset and peak. Both PIC onset and peak were significantly depolarized in SOD1 interneurons, while amplitude of the PIC was unchanged. Depolarizing current ramps were used to measure the input-output relationship of the neurons in current clamp. Inhibitory interneurons from SOD1 mice were found to have significantly higher threshold voltage than control interneurons (Fig 3E-F). This shift is likely driven by the changes in PIC. The current at firing onset, or I-ON, was not significantly changed ($p = 0.15$), similar to the current at firing offset, or I-OFF ($p = 0.07$). AHP was also significantly different in SOD1 interneurons. The duration (at half AHP amplitude) was shorter in SOD1 neurons, as shown in Fig 3H-I. Amplitude of the AHP was unchanged. While changes in the PIC and threshold indicate less excitability in SOD1 interneurons, the shortened AHP suggests an increased ability to fire at higher rates in SOD1 interneurons, a property that is associated with increased excitability. However, no changes in firing rates were detected in SOD1 interneurons. All other properties were found to be similar in SOD1 and WT glycinergic interneurons, including maximum firing rates, sag/rebound currents (I_H), action potential parameters and membrane properties (see **Table 2** for all electrical properties). See discussion for further interpretation of these findings.

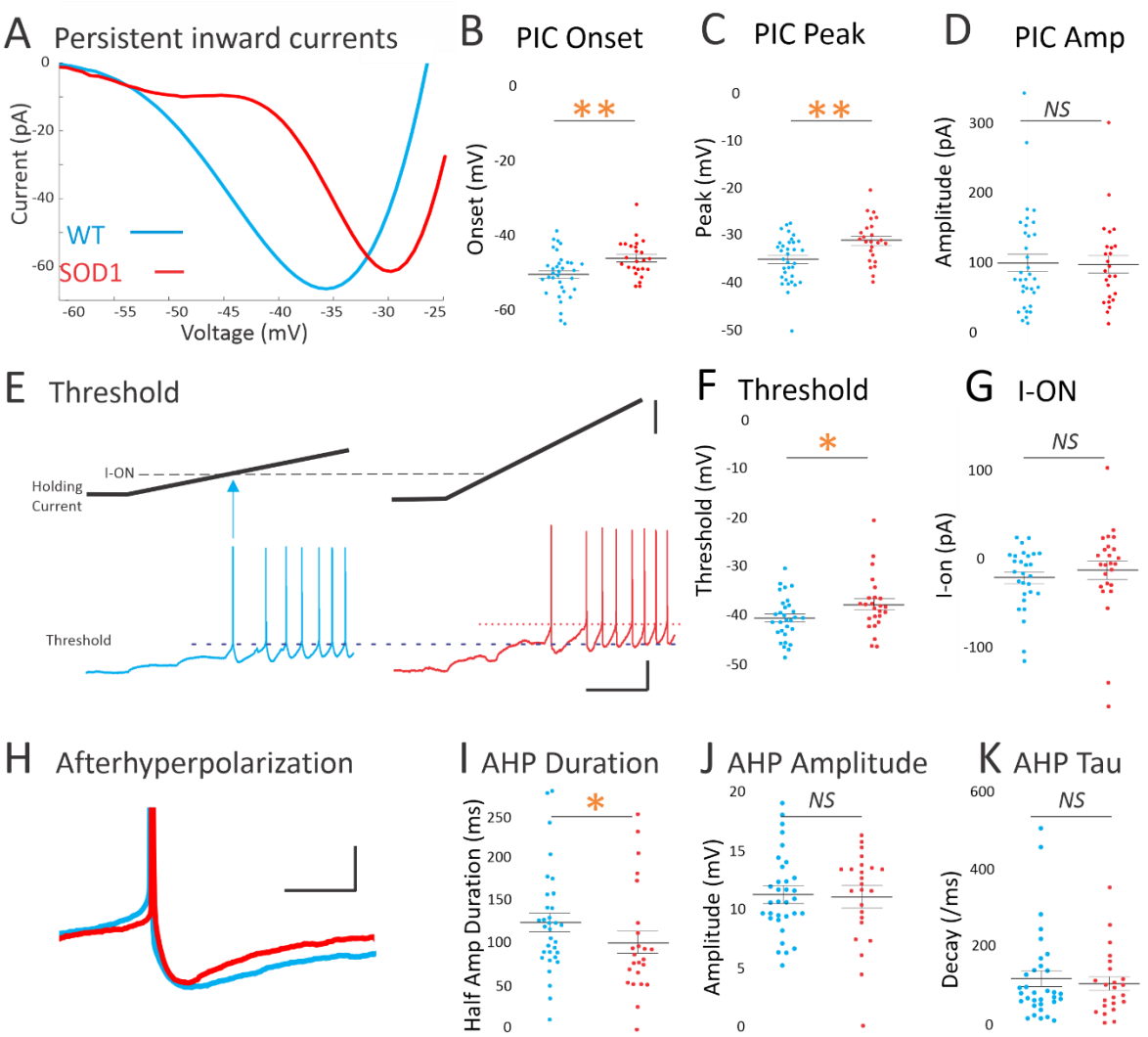

171

Figure 3: Electrophysiology of SOD1 glycinergic interneurons. The most prominent difference in SOD1 interneurons was the shift in voltage dependence of PICs and threshold. (**A**) Representative, leak-subtracted current-voltage relationship of PICs from WT (P8) and SOD1 (P6) interneurons. (**B-D**) Mean onset, peak and amplitude of PICs in WT (blue symbols on left) and SOD1 interneurons (red symbols on right). (**E-F**) Threshold voltage (action potentials evoked with current ramps as shown) was depolarized in SOD1 interneurons. Starting potential for both interneurons was -65mV. The current at firing onset (I-ON) was not significantly different as shown in **G.** (**H**) The AHP in SOD1 interneurons was shorter, as shown by the smaller mean duration at half amplitude in a representative P8 WT and P7 SOD1 interneuron and cumulative data in **I.** Neither the AHP amplitude nor the AHP decay time constant, tau, were significantly altered in SOD1 glycinergic interneurons, as shown in **J-K.** Vertical scale bars in **E**: top = 50pA, and bottom = 20mV. Horizontal scale bar in **E** = 0.5s and all scale bars apply to both left and right panels. Vertical scale bar in H = 10mV (APs were truncated from image), and horizontal scale bar = 50ms. Significance denoted with * indicates $p \leq 0.05$; ** indicates $p < 0.01$.

172

173

Table 2: Electrophysiological properties of GlyT2-GFP+ interneurons in WT and SOD1 animals.

Parameters	**Groups**		
	WT (Mean ± SE)	**SOD (Mean ± SE)**	***p***
	N = 34	*N* = 25	
Resting membrane potential (mV)	-46.7 ± 1.1	-45.7 ± 1.4	0.524[K]
Capacitance (pF)	66 ± 7	55 ± 5	0.529[K]
Input resistance (MΩ)	295 ± 32	299 ± 41	0.794[K]
PIC properties			
PIC onset (mV)	-50.5 ± 1.0	-46.2 ± 1.0**	0.004
PIC peak (mV)	-35.1 ± 0.8	-31.2 ± 0.9**	0.003
PIC amplitude (pA)	100 ± 13	97 ± 12	0.890[K]
Normalized PIC (pA/pF)	1.79 ± 0.24	1.92 ± 0.22	0.226[K]
Firing properties			
Inst firing freq range max (Hz)	112 ± 8	113 ± 8	0.961
Steady state firing freq range min (Hz)	6 ± 0.4	6 ± 0.7	0.453[K]
I-ON (pA)	-55 ± 23	-14 ± 11	0.148[K]
I-OFF (pA)	14 ± 14	36 ± 14	0.074[K]
Δ I (pA)	70 ± 14	50 ± 10	0.331[K]
AP properties			
AP overshoot past 0 (mV)	20.0 ± 1.7	21.4 ± 1.6	0.553
AP duration at half peak (ms)	1.53 ± 0.09	1.48 ± 0.08	0.944
AP rate of rise (V/s)	87 ± 5	83 ± 3	0.428[K]
AP rate of fall (V/s)	45 ± 3	43 ± 2	0.924[K]
Threshold on ramp (mV)	-40.6 ± 0.8	-37.9 ± 1.1*	0.052[K]
Threshold on step (mV)	-47.3 ± 0.8	-45.1 ± 1.3	0.199[K]
AHP properties			
AHP amplitude (mV)	11.2 ± 0.6	11.0 ± 0.8	0.704[K]
AHP duration at half amplitude (s)	0.12 ± 0.01	0.10 ± 0.01*	0.045[K]
AHP tau (s^{-1})	0.12 ± 0.02	0.10 ± 0.02	0.980[K]
I_H properties			
Hyperpolarizing Sag (%)	32 ± 3	32 ± 4	0.537[K]
Depolarizing Rebound (%)	17 ± 3	19 ± 5	0.536[K]

Significance denoted with * indicates $p \leq 0.05$; ** indicates $p < 0.01$.

[K] Indicates Kruskal-Wallis Test for nonparametric distributions; all others were ANOVA analysis.

174

175

176 **Regional analysis of glycinergic interneurons**

177 Since ventral glycinergic interneurons are not a homogenous population, we tested for regional
178 differences. Interneurons were divided into three groups based on location 1) the "ventral RC region"
179 within 100 µm of the ventral white matter where Renshaw cells are located, 2) lamina IX, and 3) the
180 "intermediate region" of the ventral horn including lamina VII and VIII, excluding the previous two
181 regions. These regions are shown in **Figure 4**. The first region corresponds to the location of RCs (but
182 could contain other types of glycinergic interneurons). The second region contains interneurons that are
183 interspersed with the MNs within the motor pools, likely to be composed of premotor interneurons
184 (more on this in the discussion). The third region contains interneurons that are a mix of premotor
185 interneurons and other classes of ventral interneurons. There was overlap of the first two regions, so
186 interneurons within the ventralmost 100um that also were located within motor pools were included in
187 both the ventral RC region and lamina IX, as shown in open circles in figure 4.

188
189

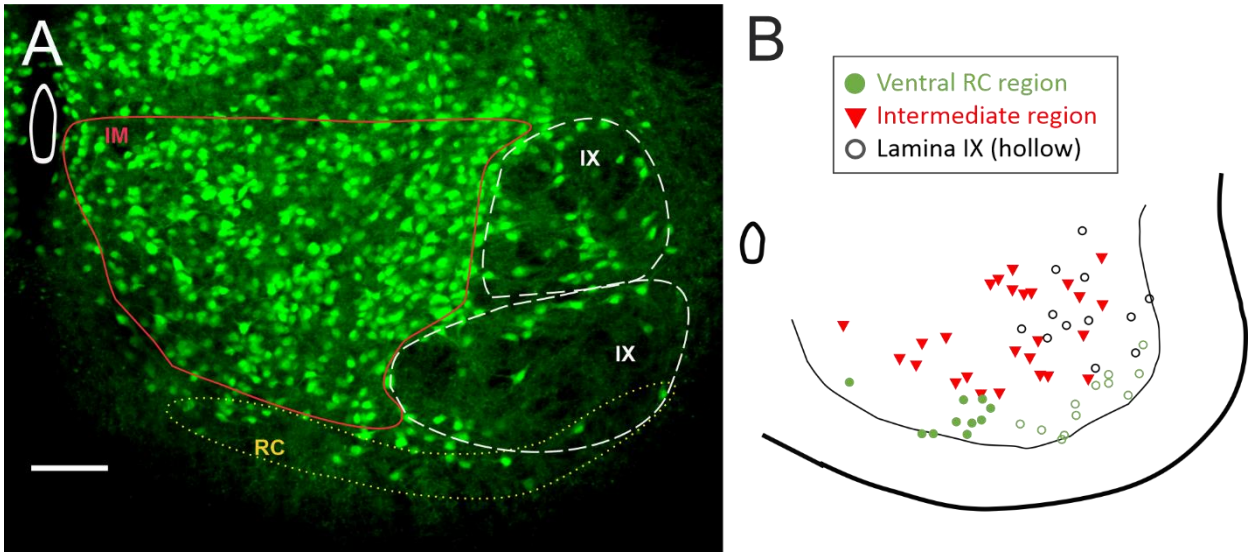

Figure 4: Regional divisions of interneurons. (**A**) Three regions were used for analysis of regional differences in glycinergic interneurons. (**B**) Map of the patched interneurons coded for regions. Ventral region with RC cells (green circles) overlapped with lamina IX (hollow circles). The remaining interneurons that were not within the RC region or lamina IX were grouped into an intermediate region of lamina VII and VIII (red triangles). Scale bar in **A** = 100 µm.

GlyT2 interneurons in Ventral RC region

Within the ventral region where RCs are located, we found that SOD1 interneurons there showed the most significant changes in both electrophysiology and morphology (particularly dendritic morphology). In patch clamped interneurons from this region (N = 8 WT from 7 mice and 13 SOD1 from 9 mice), there was a significant depolarization in PIC onset and peak in glycinergic SOD1 interneurons compared to WT interneurons in the same location. Additionally, dendrites were found to be longer and larger in volume and surface area in SOD1 interneurons in the ventral-most 100 µm. Unpatched GlyT2+ SOD1 interneurons in this region (129 WT interneurons from 8 WT mice and 168 SOD1 interneurons from 9 SOD1 mice) were smaller than WT. These changes (summarized in **Figure 5** and **Table 3**) show that glycinergic neurons in the region where RCs are located are very affected by the SOD1 mutation.

GlyT2 interneurons in Lamina IX

The SOD1 interneurons located in lamina IX, intermixed with MNs were modestly altered in excitability and morphology. As shown in **Figure 6** and **Table 4**, PIC onset was depolarized in SOD1 interneurons in this region, compared to interneurons in this region from WT mice (n = 14 WT interneurons from 8 mice and 11 SOD1 interneurons from 9 mice). Longer dendritic length was also found in patched interneurons in this region, and within the larger number of unpatched interneurons, (345 WT interneurons from 7 WT mice and 306 SOD1 interneurons from 8 SOD1 mice) SOD1 interneurons were found to have smaller somata than WT interneurons.

GlyT2 interneurons in the Intermediate region

The third regional group of glycinergic interneurons was defined as the intermediate region. These interneurons were located in laminae VII and VIII, excluding the ventral 100 µm (and of course excluding lamina IX). Within this area, 16 WT and 8 SOD1 interneurons were patched from 11 WT and 5 SOD1 mice respectively, and 2077 unpatched interneurons were analyzed from 9 WT mice and 1113 unpatched SOD1 interneurons from 9 SOD1 mice. As shown in **Figure 7** and **Table 5**, we found little was changed in electrophysiological parameters of SOD1 interneurons (only PIC peak was significantly depolarized). In unpatched neurons from this region, we found that soma size was significantly smaller in SOD1 interneurons, similar to the other two regions.

219

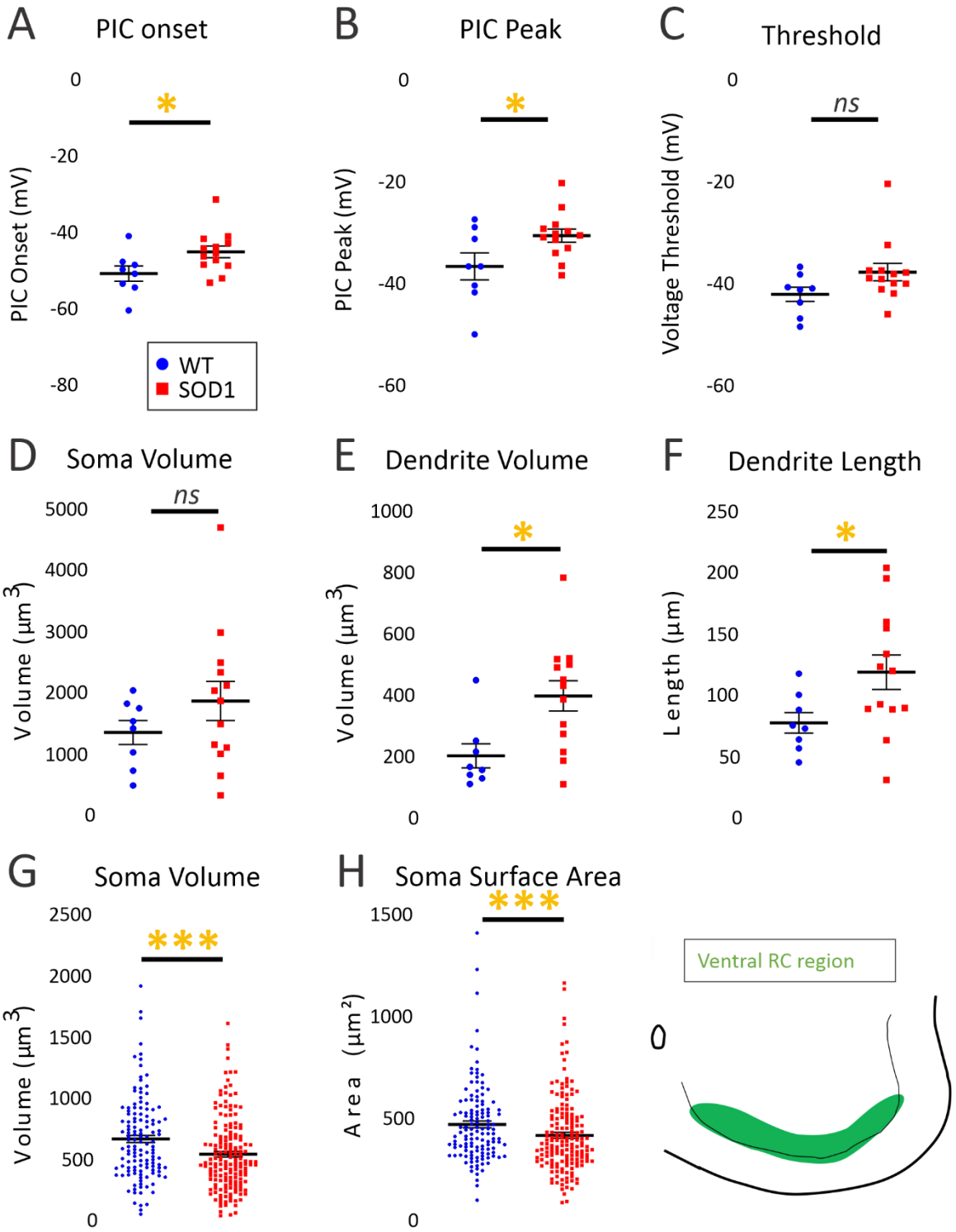

Figure 5: PICs were depolarized in SOD1 GlyT2 interneurons in the ventral RC region. Both onset (**A**) and peak (**B**) of the PIC were depolarized, but voltage threshold (**C**) was not significant. Soma volume of patched neurons (**D**) was unchanged, though dendrites of SOD1 interneurons had more volume (**E**) and were longer (**F**). Larger numbers of unpatched neurons showed smaller soma volume (**G**) and surface area (**H**) in SOD1 interneurons than WT, in RC region. Significance denoted with * indicates $p \leq 0.05$, ** indicates $p \leq 0.01$.

220

221

222

Table 3: Electrophysiological properties of GlyT2-GFP+ interneurons in WT and SOD1 animals in ventral RC region.

	WT (Mean ± SE)	SOD (Mean ± SE)	*p*
	N = 8	N = 13	
PIC Onset (mV)	-51.3 (± 2.0)	-45.6 (± 1.5) *	0.036
PIC Peak (mV)	-36.8 (± 2.6)	-30.8 (± 1.3) *	0.034
PIC Amplitude (pA)	77.2 (± 15.6)	114.9 (± 19.7)	0.218[K]
I-ON (pA)	-65.6 (± 39.0)	-18.1 (± 14.2)	0.096[K]
I-OFF (pA)	-31.9 (± 20.5)	6.9 (± 15.0)	0.060[K]
Δ I (pA)	36.3 (± 19.4)	25.1 (± 6.8)	0.717[K]
Threshold on ramp (mV)	-42.4 (± 1.4)	-38.0 (± 1.7)	0.070[K]
Threshold on step (mV)	-47.0 (± 1.1)	-44.1 (± 1.6)	0.261[K]
AHP amplitude (mV)	11.6 (± 1.4)	11.4 (± 1.0)	0.921
AHP duration at half amplitude (s)	0.128 (± 0.027)	0.117 (± 0.016)	0.469[K]
AHP tau (s^{-1})	0.117 (± 0.050)	0.109 (± 0.020)	0.346[K]
Morphology of Patched interneurons in RC region			
	N = 8	N = 13	
Soma Surface Area (μm^2)	589.4 (± 59.0)	700.0 (± 79.1)	0.334
Soma Volume (μm^3)	1326.0 (± 195.4)	1841.0 (± 318.8)	0.253
Dendrite Length (µm)	76.4 (± 8.4)	117.7 (± 14.0) *	0.044
Dendrite Surface Area (μm^2)	407.6 (± 57.3)	680.7 (± 65.7) *	0.011[K]
Dendrite Volume (μm^3)	196.3 (± 38.9)	391.5 (± 49.7) *	0.014[K]
Morphology of Unpatched interneurons in RC region			
	N = 129	N = 168	
Soma Surface Area (μm^2)	466.2 (± 17.0)	412.3 (± 14.4) ***	0.000[K]
Soma Volume (μm^3)	657.2 (± 29.7)	532.8 (± 23.2) ***	0.000[K]

Significance denoted with * indicates $p \leq 0.05$; *** indicates $p < 0.001$.

[K] Indicates Kruskal-Wallis Test for nonparametric distributions; all others were ANOVA analysis.

223

224

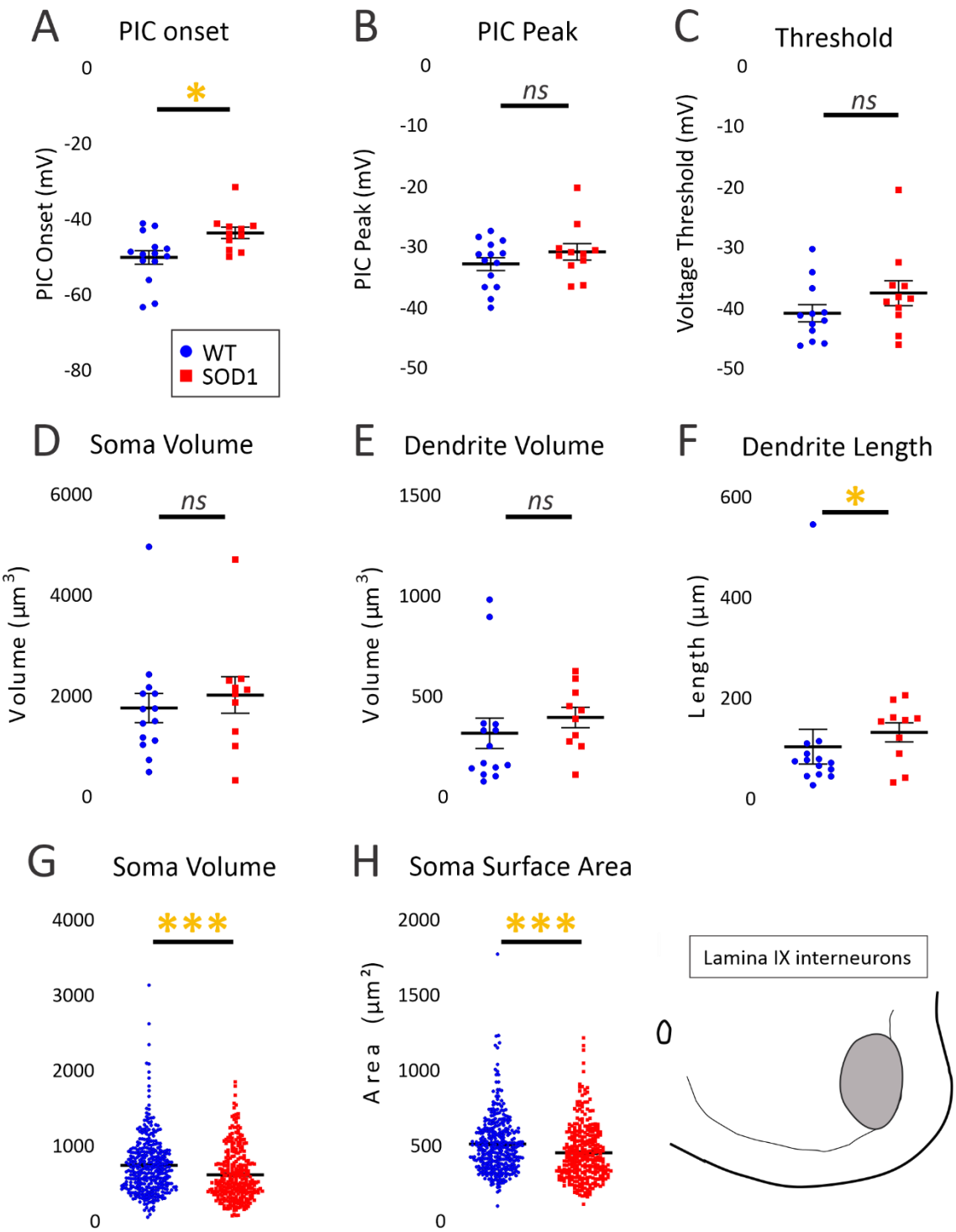

Figure 6: Electrophysiology and morphology was altered in glycinergic SOD1 interneurons in lamina IX. PIC onset (**A**), PIC peak (**B**) and voltage threshold (**C**) were all depolarized in SOD1 interneurons. Soma (**D**) and dendrites (**E**) and (**F**) of patched SOD1 interneurons were unchanged. Larger numbers of unpatched neurons showed smaller soma volume (**G**) and surface area (**H**) in SOD1 interneurons than WT in Lamina IX. Significance denoted with * indicates $p \leq 0.05$, *** indicates $p \leq 0.001$.

226
227

Table 4: Electrophysiological properties of GlyT2-GFP+ interneurons in WT and SOD1 animals in lamina IX.

	WT (Mean ± SE)	**SOD (Mean ± SE)**	***p***
	N = 14	N = 11	
PIC Onset (mV)	-50.5 (± 1.8)	-44.0 (± 1.5) *	0.013
PIC Peak (mV)	-33.1 (± 1.1)	-31.1 (± 1.4)	0.248
PIC Amplitude (pA)	115.9 (± 21.7)	98.1 (± 22.8)	0.412[K]
I-ON (pA)	-78.3 (± 47.0)	-11.3 (± 19.3)	0.155[K]
I-OFF (pA)	21.9 (± 27.9)	22.2 (± 22.0)	0.250[K]
Δ I (pA)	101.7 (± 73.1)	33.4 (± 9.0)	0.701
Threshold on ramp (mV)	-41.1 (± 1.4)	-37.8 (± 2.1)	0.193
Threshold on step (mV)	-47.4 (± 1.1)	-43.9 (± 2.2)	0.112[K]
AHP amplitude (mV)	11.4 (± 1.0)	10.2 (± 1.0)	0.421
AHP duration at half amplitude (s)	0.125 (± 0.019)	0.094 (± 0.019)	0.139[K]
AHP tau (s^{-1})	0.129 (± 0.032)	0.076 (± 0.032)	0.274[K]
Morphology of Patched interneurons in lamina IX			
	N = 14	N = 10	
Soma Surface Area (μm^2)	702.6 (± 77.5)	734.3 (± 89.8)	0.771
Soma Volume (μm^3)	1731.2 (± 288.6)	1988.8 (± 363.2)	0.412[K]
Dendrite Length (µm)	100.8 (± 34.6)	129.3 (± 18.9) *	0.046[K]
Dendrite Surface Area (μm^2)	544.8 (± 140.1)	721.5 (± 92.8)	0.089[K]
Dendrite Volume (μm^3)	308.8 (± 75.5)	387.6 (± 51.0)	0.114[K]
Morphology of Unpatched interneurons in lamina IX			
	N = 345	N = 306	
Soma Surface Area (μm^2)	505.9 (± 10.4)	448.3 (± 10.7) ***	0.000[K]
Soma Volume (μm^3)	732.0 (± 21.1)	605.1 (± 19.6) ***	0.000[K]

Significance denoted with * indicates $p \leq 0.05$; *** indicates $p < 0.001$.

[K] Indicates Kruskal-Wallis Test for nonparametric distributions; all others were ANOVA analysis.

228
229

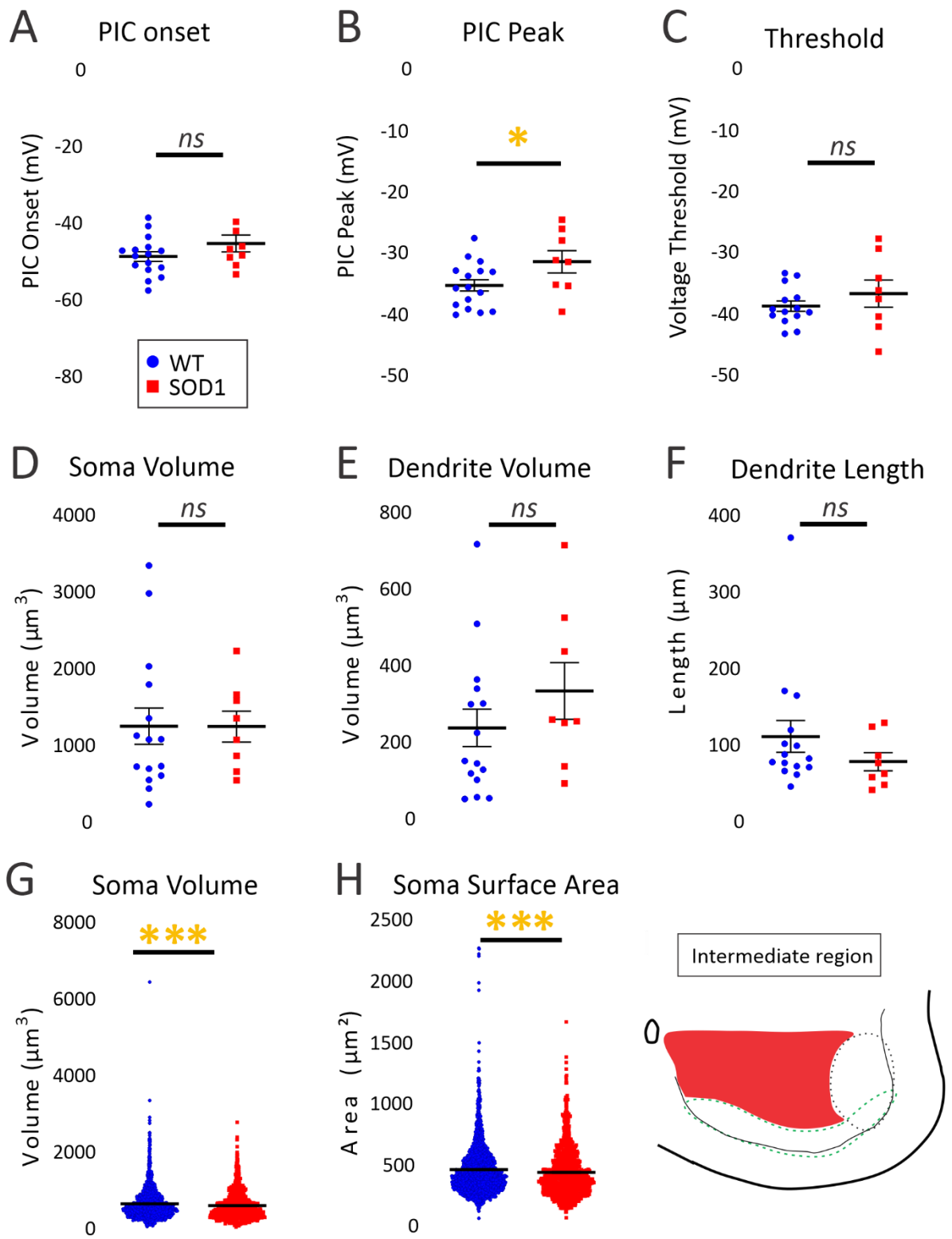

Figure 7: Morphology was altered in SOD1 interneurons in the intermediate regions of laminae VII and VIII. PIC onset (**A**) was not significantly different in SOD1 interneurons, though PIC peak (**B**) was depolarized. Voltage threshold (**C**) was not affected in SOD1 interneurons. Morphology of soma (**D**) and dendrites (**E**) in patched SOD1 interneurons were unchanged, however larger numbers of unpatched neurons showed smaller soma volume (**G**) and surface area (**H**) in SOD1 interneurons than in WT, in laminas VII and VIII. Significance denoted with * indicates $p \leq 0.05$, *** indicates $p \leq 0.001$.

231

232 **Table 5**: Electrophysiological properties of GlyT2-GFP+ interneurons in WT and SOD1 animals in Intermediate Region of lamina VII and VIII.

Parameters	**Groups**		
	WT (Mean ± SE)	**SOD (Mean ± SE)**	***p***
	N = 16	N = 8	
PIC Onset (mV)	-49.0 (± 1.3)	-47.4 (± 1.6)	0.435
PIC Peak (mV)	-35.5 (± 0.9)	-31.7 (± 1.8) *	0.046
PIC Amplitude (pA)	92.1 (± 16.7)	77.0 (± 17.7)	0.881[K]
I-ON (pA)	-18.2 (± 11.6)	-16.5 (± 19.1)	0.776[K]
I-OFF (pA)	20.9 (± 12.2)	73.9 (± 26.7)	0.101[K]
Δ I (pA)	39.0 (± 9.1)	69.1 (± 24.4)	0.076[K]
Threshold on ramp (mV)	-38.9 (± 0.83)	-37.0 (± 2.2)	0.525[K]
Threshold on step (mV)	-46.7 (± 1.2)	-46.3 (± 2.4)	0.490[K]
AHP amplitude (mV)	11.3 (± 0.8)	10.5 (± 2.0)	0.658
AHP duration at half amplitude (s)	0.116 (± 0.011)	0.095 (± 0.030)	0.267[K]
AHP tau (s^{-1})	0.119 (± 0.032)	0.127 (± 0.051)	1.000[K]
Morphology of Patched interneurons in laminae VII and VIII.			
	N = 15	N = 8	
Soma Surface Area (μm^2)	573.5 (± 62.9)	558.5 (± 56.7)	0.699[K]
Soma Volume (μm^3)	1232.3 (± 237.4)	1228.2 (± 201.6)	0.776[K]
Dendrite Length (μm)	109.7 (± 20.7)	76.7 (± 11.7)	0.238[K]
Dendrite Surface Area (μm^2)	505.5 (± 83.0)	513.7 (± 93.6)	0.728[K]
Dendrite Volume (μm^3)	233.9 (± 48.8)	330.4 (± 74.1)	0.294[K]
Morphology of Unpatched interneurons in laminae VII and VIII.			
	N = 2077	N = 1113	
Soma Surface Area (μm^2)	451.7 (± 4.6)	428.3 (± 5.9) ***	0.000[K]
Soma Volume (μm^3)	624.9 (± 9.0)	575.3 (± 11.4) ***	0.000[K]

Significance denoted with * indicates $p \leq 0.05$; *** indicates $p < 0.001$.

[K] Indicates Kruskal-Wallis Test for nonparametric distributions; all others were ANOVA analysis.

233

234

Taken together, these results show that glycinergic interneurons are profoundly affected by the SOD1 mutation and are altered very early in life in both electrophysiology and morphology. These changes are not universal to all glycinergic interneurons, but rather are specific to various subtypes of inhibitory interneurons.

Discussion

This study shows for the first time that glycinergic interneurons are depressed in excitability in the SOD1 mouse model and may be contributing to ALS pathology. Alterations in both morphology and excitability of glycinergic interneurons occur at a very early stage. GlyT2 interneurons in SOD1 mice are smaller and depressed in excitability, particularly those within 100um of the ventral white matter, as summarized in **Figure 8**. We speculate that these shifts in interneuron excitability and morphology could have functional consequences that alter inhibition of MNs, modify motor output, and may even provide an early biomarker of ALS.

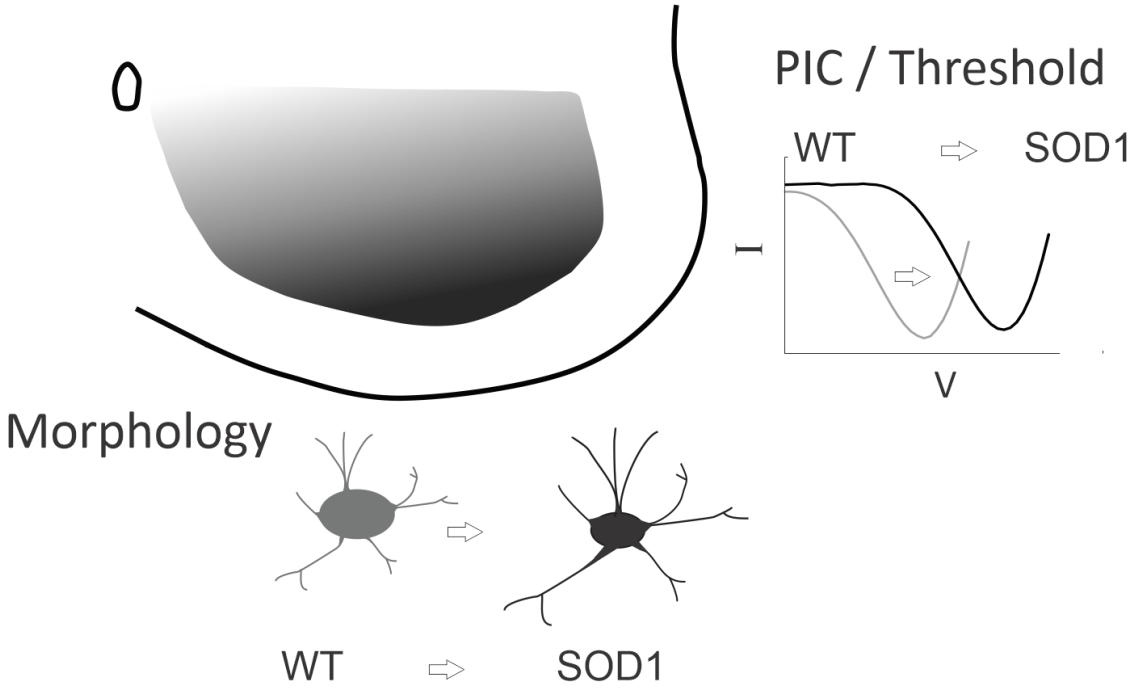

Figure 8: SOD1 GlyT2 interneurons are most profoundly altered in the ventral-most 100µm of the spinal cord, the area where Renshaw cells are found. All ventral interneurons showed changes in morphology and excitability, including depolarization of PICs and smaller somata. Interneurons in the ventral region and lamina IX showed increased dendritic length. Interneurons in the ventral region had the most strongly affected electrophysiology (both PIC onset and peak depolarized).

250 *Intrinsic and synaptic hyperexcitability*

251 A core issue this study brings to light is potential long-term disruption to the balance of excitatory and
252 inhibitory synaptic transmission in ALS. Spinal cord and cortex both show an imbalance between
253 excitatory and inhibitory synaptic transmission in SOD^{G93A} mice (Avossa et al., 2006; Saba et al., 2016).
254 Clinically, ALS patients show evidence of altered synaptic activity as well, including a reduction in
255 inhibition. A reduction of glycinergic receptor binding in the anterior gray matter of the spinal cord
256 (Hayashi et al., 1981; Whitehouse et al., 1983) has been demonstrated along with abnormal glycine and
257 gamma amino butyric acid (GABA) levels in blood serum (Malessa et al., 1991; Niebroj-Dobosz and Janik,
258 1999). Electrophysiology also suggests disruption in spinal inhibitory circuits in ALS patients (Raynor and
259 Shefner, 1994; Shefner and Logigian, 1998; Sangari et al., 2016; Özyurt et al., 2020). An interesting
260 question is whether the neurons are altered in excitability only within the motor circuit (i.e. corticospinal
261 neurons and the synaptically-connected spinal inhibitory and cholinergic interneurons, and MNs), or if
262 disturbances are more widespread throughout the nervous system. In the spinal cord, interneurons that
263 serve as conduits between vulnerable corticospinal and spinal MNs include cholinergic interneurons, Ia
264 inhibitory interneurons and RCs. There is abundant evidence of disruption in these cholinergic,
265 GABAergic and glycinergic synapses from animal models (Martin et al., 2007; Chang and Martin, 2009b;
266 Pullen and Athanasiou, 2009; Hossaini et al., 2011; Herron and Miles, 2012; Casas et al., 2013; Wootz et
267 al., 2013; Saxena et al., 2013; Milan et al., 2015; Dukkipati et al., 2016; Medelin et al., 2016). Similarly, in
268 the cortex, neurons that are not themselves vulnerable to neurodegeneration in ALS also exhibit altered
269 excitability and morphology in a parallel time course to the vulnerable corticospinal neurons (Clark et al.,
270 2017, 2018; Kim et al., 2017). The changes in excitability of other neuronal populations must contribute
271 to the imbalance of both excitatory and inhibitory neurotransmission that has been clearly
272 demonstrated in ALS patients and animal models.

273 A case for hyperexcitability and glutamate excitotoxicity involvement in ALS pathogenesis has been
274 more controversial. Altered intrinsic excitability has been consistently reported in both corticospinal
275 projection neurons and spinal MNs, but these perturbations appear to fluctuate based on age/disease
276 progression. Corticospinal projection neurons have increased firing and other signs of hyperexcitability
277 during the first week of postnatal development (Pieri et al., 2009; Saba et al., 2016, 2019; Kim et al.,
278 2017), but excitability is normal in young and adult pre-symptomatic ages (Kim et al., 2017; Saba et al.,
279 2019), and may become hypoexcitable at the age of symptom onset (Saba et al., 2019). Similarly, spinal
280 MNs show intrinsic hyperexcitability at very early (embryonic) stages (Kuo et al., 2004, 2005; Martin et

281 al., 2013). At a postnatal age similar to the inhibitory interneurons in this study, spinal MNs do *not* have
282 an altered threshold, rheobase or frequency-current relationship, though other abnormalities are
283 present in PICs, action potential duration, AHP and dendritic Ca^{2+} entry (Pambo-Pambo et al., 2009;
284 Quinlan et al., 2011, 2015; Leroy et al., 2014). Thus, at the age studied here, *inhibitory interneurons are*
285 *more disrupted in excitability than the vulnerable spinal MNs*. At symptom onset, MNs may finally
286 succumb to hypoexcitability, though not all studies agree on this point (Delestrée et al., 2014; Martinez-
287 Silva et al., 2018; Jensen et al., 2020). Notably, MNs derived from ALS patients' induced pluripotent stem
288 cells also show initial hyperexcitability followed by hypoexcitability (Wainger et al., 2014; Devlin et al.,
289 2015), and increasing excitability of MNs enhanced neuroprotection rather than neurodegeneration
290 (Saxena et al., 2013). A unifying theme throughout the findings is that vulnerable MNs show excessive
291 homeostatic gain in response to perturbation (Kuo et al., 2020), and not only excitability but other
292 cellular properties fluctuate over the lifespan of the animal (Irvin et al., 2015). In light of that, whether
293 inhibitory interneurons are less excitable at other ages should be explored in future studies to fully
294 characterize their contribution to neurodegenerative processes.
295 *Changes in neuron morphology*
296 In ALS models, altered morphology in spinal MNs occurs so early that it could be viewed as a deficit in
297 normal development. Embryonically, SOD1 MNs have shorter projections but this is reversed during
298 postnatal development. At 1-2 weeks of age, MNs begin to show more dendritic branching and larger
299 soma sizes (Amendola and Durand, 2008; Filipchuk and Durand, 2012; Martin et al., 2013). Interestingly,
300 this could be caused by lack of inhibitory input to MNs (Fogarty et al., 2016). Spinal MNs remain larger
301 through adulthood (Dukkipati et al., 2018). In contrast to the spinal MNs at this age, we found that
302 inhibitory interneurons had smaller soma size and yet had expanded dendritic surface area and volume.
303 This is reminiscent of changes in corticospinal neurons: presymptomatic corticospinal neurons also have
304 increased arborization but with smaller soma diameters (Ozdinler et al., 2011; Saba et al., 2016). In both
305 sporadic and familial ALS patients, postmortem tissue shows degeneration of apical dendrites in
306 corticospinal neurons and smaller soma size (Genç et al., 2017). In the spinal interneurons, increased
307 dendrite length, surface area and volume occurs in specific populations of interneurons: the increased
308 dendritic arbor is specifically found in the ventral interneurons, while the smaller soma sizes are more
309 universal. Increased neuronal size / arborization over the life span could greatly increase the impact of
310 other stressors (e.g., proteostasis, metabolic deficits, intracellular transport) on vulnerable neuron
311 populations.

312 *After spike afterhyperpolarization*

313 The AHP can contribute to a neuron's firing rate such that a neuron with a large, long-lasting AHP will
314 typically fire at a slower rate (typical of slow/type I MNs) than a neuron with small, fast-decaying AHP
315 (typical of fast/type II MNs). In ALS patients, the AHP is shortened in MNs of patients with little force
316 deficits and later elongated in patients with large force deficits (Piotrkiewicz and Hausmanowa-
317 Petrusewicz, 2011), which could reflect early changes in physiology of vulnerable fast MNs and later, the
318 remaining, less-vulnerable population of slow MNs. Similarly, SOD1 mouse MNs show shorter AHPs
319 early, and longer AHPs around symptom onset (Quinlan et al., 2011; Jensen et al., 2020). Here we show
320 that AHP is shorter in duration in SOD1 interneurons very early in life. In the regional analysis, AHP
321 parameters were not found to be significantly altered in any of the 3 regions, but it is possible this was
322 due to a loss in statistical power in the smaller groups. We did not find concomitant changes in
323 minimum or maximum firing rates in GlyT2 interneurons, so the physiological importance of the altered
324 AHP in interneurons is unclear.

325

326 *Inhibitory interneurons: Subtype specific effects*

327 The interneurons in this study were heterogenous, and based on their location and electrophysiology,
328 they likely were composed of V1 and V2b interneurons including RCs, commissural interneurons (V2b
329 interneurons), and Ia inhibitory interneurons, and perhaps inhibitory propriospinal interneurons (Willis
330 and Willis, 1964; Restrepo et al., 2009; Bikoff et al., 2016; Flynn et al., 2017). Because of this
331 heterogeneity, interneurons were separated into regions for further analysis, to examine more
332 specifically which inhibitory interneurons were perturbed. Based on our regional analysis, interneurons
333 in the ventral-most 100um were altered the most in excitability, with the most strongly depolarized
334 PICs, moreso than the glycinergic interneurons within lamina IX and intermediate lamina VI and VII.
335 Interneurons located in the region within 100µm from the ventral white matter likely contain RCs based
336 on the location (Siembab et al., 2010) and electrophysiological characteristics (Perry et al., 2015; Bikoff
337 et al., 2016). Glycinergic interneurons located in lamina IX are reminiscent of the locomotor-related
338 GABAergic interneurons characterized by Nishimaru and colleagues, which were located within the
339 ventrolateral spinal cord, surrounded MNs and were active during locomotor activity (Nishimaru et al.,
340 2011). Indeed these may be the same neurons: colocalization of GABA and glycine is entirely possible
341 (Jonas et al., 1998; Allain et al., 2006). If the lamina IX interneurons are indeed locomotor-related, even
342 a modest dampening of excitability observed here in SOD1 mice could contribute to changes in

343 locomotor patterning as has been described in other studies (Quinlan et al., 2017; Allodi et al., 2021).
344 Further studies are warranted to examine how inhibitory interneurons may be differently modulated in
345 a subtype-specific manner in animal models of ALS.
346
347 *Functional implications for impaired inhibitory circuits*
348 Outward signs of improperly functioning inhibitory interneurons may be apparent from subtle changes
349 in motor patterning and could potentially be used as a biomarker of early ALS. Locomotor disturbances
350 have been demonstrated *in vivo* in presymptomatic SOD1 mice during walking/running (Vinsant et al.,
351 2013a, 2013b; Akay, 2014; Quinlan et al., 2017; Allodi et al., 2021). In the embryonic and neonatal spinal
352 cord *in vitro*, increased duration of depolarizing events in MNs and a slower period of locomotor-related
353 bursting has been described (Medelin et al., 2016; Branchereau et al., 2019), which indicate that even
354 during development the functioning of locomotor circuits is already impaired. In presymptomatic adult
355 mice capable of running on a treadmill, subtle locomotor differences are observed including advanced
356 intermuscular phasing and a slower speed (Quinlan et al., 2017; Allodi et al., 2021) which indicate that
357 before any large scale neurodegeneration occurs, there are changes in patterns of activity in MNs and
358 interneurons that could be exploited for use as a biomarker of ALS. At initial symptom onset, the first
359 failure of the tibialis anterior manifests as abnormality in the swing phase of the ankle (Akay, 2014).
360 Interestingly, silencing different interneuron populations (including inhibitory interneurons and
361 cholinergic interneurons) reveals the contribution of each population: silencing cholinergic interneurons
362 increases locomotor deficits in SOD1 mice (Landoni et al., 2019), while silencing inhibitory interneurons
363 has no effect suggesting these interneurons are already impaired (Allodi et al., 2021).
364
365 *Clinical-translational implications*
366 Evidence of MN hyperexcitability in ALS patients is present alongside signs of dysfunction in inhibition
367 (Rothstein et al., 1992; Plaitakis and Constantakakis, 1993; Raynor and Shefner, 1994; Shefner and
368 Logigian, 1998; Andreadou et al., 2008; Bae et al., 2013). Perhaps reducing excitability (with riluzole, for
369 example) only results in a modest increase in lifespan (Bensimon et al., 1994) because it could be helpful
370 to MNs while exacerbating inhibitory dysfunction by further depressing excitability of inhibitory
371 interneurons like RCs. Thus, a more targeted approach to reduce MN excitability could be beneficial
372 early in disease pathology. Stimulation of inhibitory nerves or certain protocols of transcranial
373 stimulation could be explored, along with augmentation of inhibitory neurotransmission.

374 **Materials and Methods**

375 **Ethics Statement**

376 Experiments were performed in accordance with the United States National Institutes of Health Guide for
377 Care and Use of Laboratory Animals. Approval of the Northwestern University's Animal Care and Use
378 Committee was obtained for all experiments performed in this study. All efforts were made to minimize
379 animal suffering and to reduce the number of animals used.

380 **Animals and Tissue harvest**

381 Transgenic B6SJL mice overexpressing the human *SOD1*^{G93A} gene (strain 002726, Jackson Labs, Bar Harbor,
382 ME, USA) and their wild type littermates were used (nontransgenic for the human *SOD1*^{G93A} gene).
383 Transgenic animals were identified using standard PCR techniques by Transnetyx (Cordova, TN, USA) and
384 were bred with GlyT2-eGFP mice (Zeilhofer et al., 2005) generating SOD1^{G93A} GlyT2-eGFP mice, here called
385 SOD1. Inhibitory glycinergic interneurons express the Na^+ and Cl^- coupled glycine transporter 2, or GlyT2.
386 GlyT2-eGFP expression is driven by the GlyT2 promotor. Specifically, GlyT2-eGFP females were bred with
387 SOD1^{G93A} GlyT2-eGFP males, and progeny were used for experiments without knowing if they were
388 SOD1^{G93A} GlyT2-eGFP or GlyT2-eGFP. Genotyping was performed post-experimentally. For the following
389 studies juvenile mouse pups were used between postnatal day (P) 6 - 10. Mice were deeply anesthetized
390 with isoflurane (Henry Schein Animal Health, Dublin, OH, USA), decapitated and eviscerated. The lumbar
391 spinal cord from L1 - L6 was removed and embedded in 2.5% w/v agar (No. A-7002, Sigma-Aldrich, St
392 Louis, MO, USA). The agar block was then superglued with Loctite 401 (Henkel Corporation, Rocky Hill,
393 CN, USA) to a stainless steel slicing chuck and 350 µm transverse slices were made using the Leica 1000
394 vibratome (Leica Microsystems, Buffalo Grove, IL, USA) as described previously (Quinlan et al., 2011).
395 During both spinal cord isolation and slicing, the spinal cord was immersed in 1–4°C high osmolarity
396 dissecting solution containing (mM): sucrose 234.0, KCl 2.5, $CaCl_2 \cdot 2H_2O$ 0.1, $MgSO_4 \cdot 7H_2O$ 4.0, HEPES
397 15.0, glucose 11.0, and Na_2PO_4 1.0. The pH was adjusted to 7.35 when bubbled with 95% O_2/5% CO_2 using
398 1 M KOH (Fluka Analytical, Sigma-Aldrich). After cutting, the slices were incubated for >1 h at 30°C in
399 incubating solution containing (mM): NaCl 126.0, KCl 2.5, $CaCl_2 \cdot 2H_2O$ 2.0, $MgCl_2 \cdot 6H_2O$ 2.0, $NaHCO_3$ 26.0,
400 glucose 10.0, pH 7.4 when bubbled with 95% O_2/5% CO_2 (all reagents for solutions were purchased from
401 Sigma-Aldrich).

402 **Morphological analysis**

403 Neuron morphology was assessed from two types of images: 1) 2-photon image z-stacks of live neurons
404 taken immediately after obtaining electrophysiological parameters, and 2) confocal image stacks taken
405 after fixation and tissue processing. Images collected using these two methods were analyzed

406 separately. Measurements from 2-photon images included measurements from both soma and
407 dendrites (soma volume, soma surface area, and average dendrite length, dendrite surface area and
408 dendrite volume). Data from confocal images only included soma measurements, specifically soma
409 volume and soma surface area. The reconstruction is made based on the sum of many sections of image
410 (z stacks), resulting in the 3D image. Volume is computed by sum of each section area, multiplied by the
411 thickness, resulting in the volume; the sum of each section perimeter of the reconstruction multiplied by
412 the thickness, resulting in the surface; dendrites analysis, computed by modeling as the previous ones
413 using each piece of each branch as a frustum.
414 *Two-photon imaging:* An Olympus BX-51WIF microscope fitted with an Olympus 40x/0.8NA water-
415 dipping objective lens was used. Two-photon excitation fluorescence microscopy was performed with a
416 galvanometer-based Coherent Chameleon Ultra II laser (Coherent, Santa Clara, CA, USA) tuned to 900
417 nm. A red Bio-Rad 2100MPD photomultiplier tube (Bio-Rad, Hercules, CA, USA) (570 – 650 nm) was used
418 to collect emission in the red channel. Z-stacks were obtained for each interneuron at 1024 x 1024 pixels
419 (308 x 308 µm) resolution and roughly 100 µm in depth (step size 1 µm). From these Z-stacks, Texas
420 Red® -filled neurons were three-dimensionally reconstructed using Neurolucida software (MBF
421 Bioscience, Williston, VT, USA).
422 *Confocal imaging:* Sections were observed with a confocal laser microscope (LSM510, Zeiss,
423 Oberkochen, Darmstadt, Germany) with argon (488 nm) and helium-neon (543 nm) lasers and a 20X
424 objective. From these Z-stacks, GlyT2 positive interneurons were three-dimensionally reconstructed
425 using Neurolucida software (MBF Bioscience, Williston, VT, USA). Dimensions of neurons in each image
426 stack were averaged before compiling numbers. Total numbers of analyzed interneurons was 3,902
427 composed of 1918 neurons from 36 WT image stacks and 1984 interneurons from 44 SOD1 image
428 stacks.
429 **Electrophysiology**
430 Whole cell patch clamp was performed on MNs from the lumbar segments using 2–4 MΩ glass electrodes
431 pulled from glass capillary tubes (Item #TW150F-4, World Precision Instruments, Sarasota, FL, USA) with
432 a Flaming-Brown P-97 (Sutter Instrument Company, Novato, CA, USA). Electrodes were positioned using
433 a Sutter Instrument MP-285 motorized micromanipulator (Sutter Instrument Company). Whole-cell patch
434 clamp measurements were performed at room temperature using the Multiclamp700B amplifier
435 (Molecular Devices, Burlingame, CA, USA) and Winfluor software (University of Strathclyde, Glasgow,
436 Scotland). Briefly, slices were perfused with a modified Ringer's solution containing (in mM): 111 NaCl,

437 3.09 KCl, 25.0 $NaHCO_3$, 1.10 KH_2PO_4, 1.26 $MgSO_4$, 2.52 $CaCl_2$, and 11.1 glucose. The solution was
438 oxygenated with 95% O_2/5% CO_2 and the perfusion rate was 2.5 – 3.0 ml/min. Patch electrodes contained
439 (in mM) 138 K-gluconate, 10 HEPES, 5 ATP-Mg, 0.3 GTP-Li and Texas Red dextran (150 µM, 3000 MW,
440 from Invitrogen, Life Technologies, Grand Island, NY, USA). In voltage-clamp mode, fast and slow
441 capacitance transients, as well as whole-cell capacitance, were compensated using the automatic
442 capacitance compensation on the Multiclamp. Whole cell capacitance was recorded from the Multiclamp.

443 **Electrophysiological analysis**

444 Holding potential was set at −90 mV, and neurons were subjected to slow, depolarizing voltage ramps of
445 22.5 mV s^{-1}, bringing the cell to 0 mV in 4 s, and then back to the holding potential in the following 4 s. In
446 current clamp, neurons were subjected to depolarizing current ramps for testing I-on (the current level at
447 firing onset), I-off (the current level at cessation of firing), and the slope of the frequency–current
448 relationship. The difference between I-on and I-off is calculated for ΔI. Negative current was often
449 necessary to prevent action potential (AP) firing. Resting membrane potential was recorded as the
450 potential when 0 current was injected. Persistent inward current (PIC) parameters were measured after
451 subtraction of leak current. Onset was defined as the voltage at which the current began to deviate from
452 the horizontal, leak-subtracted trace. PIC peak was the voltage at which the PIC reached peak amplitude.
453 The linear portion of leak current (usually between -90 and -75 mV) was used to calculate whole cell input
454 resistance. The first action potential in the train evoked by a depolarizing current ramp in current clamp
455 mode was used to measure all parameters relating to action potentials. Threshold voltage was defined as
456 the voltage at which the slope exceeded 10 V/s. Threshold for action potential firing was tested in two
457 ways. The first was to use the voltage at firing onset from the current ramps up to 130 pA/s (in current
458 clamp). The second was the voltage at which a single action potential could be evoked with a current step.
459 Action potential overshoot is the voltage past 0 mV the first spike reaches. Duration of the action potential
460 is measured at half of action potential height (height is defined as overshoot – threshold voltage). Rates
461 of rise and fall are defined as the peak and the trough of the first derivative of the action potential profile.
462 Instantaneous firing frequency range max was the maximum firing rate that could be evoked from a
463 neuron. It was measured from the first or second firing frequencies on a large (>150pA) depolarizing step.
464 Steady state firing freq range minimum was the lowest firing frequency evoked from a small (~50pA)
465 depolarizing step. Hyperpolarizing steps were used to measure IH. The sag and rebound were measured
466 from largest evoked response. Sag potential was calculated as a % of the total amplitude of the
467 hyperpolarization. If a spike was evoked on rebound, the voltage threshold was used for measurement.

468 AHP duration was measured from a single spike fired during a period in which the membrane potential
469 was stable. Amplitude was measured as the downward deflection from the membrane potential. Duration
470 of the AHP was measured from the falling phase of the spike at baseline potential to the time of recovery
471 to baseline membrane potential. Half amplitude duration was measured as the duration at half of the
472 measured AHP amplitude from the falling phase of the spike at baseline potential. Tau is measured as the
473 rate of decay from the last third of the AHP.

474 **Neuron Selection**

475 Glycinergic interneurons were visually selected for recording based on 1) expression of GFP, and 2)
476 location near the MN pools. Neurons that did not repetitively fire or did not maintain a resting membrane
477 potential below -35 mV were excluded from electrophysiological analysis. Neurons that were not clearly
478 stained with Texas Red after patch clamp and/or could not be imaged clearly were not included in
479 anatomical analysis.

480 **Regional grouping**

481 Photos were taken of position of the patch electrode within the spinal cord slices after recording was
482 complete. These photos were used to recreate a map of the position of the interneurons. Interneurons
483 within the ventralmost region of the spinal cord (within 100µm of the ventral white matter) were
484 grouped into the RC region described previously (Siembab et al., 2010). Neurons that were observed to
485 be located within and on the lateral edges of the motor pools (in between motoneuron and the white
486 matter) were classified as lamina IX interneurons. Since the location of the motor pools varied
487 throughout the lumbar enlargement, this classification was determined by examination of the z stacks
488 and photos. Neurons that were not found within lamina IX and were not within the ventral RC region
489 were grouped as the intermediate region of Lamina VII/VIII.

490 **Statistical analysis**

491 The assumptions of homogeneity of variances and the normality of the distribution of values for each
492 measured characteristic were evaluated with Levine's and Shapiro-Wilk tests, respectively. Group
493 comparisons (WT vs SOD1) were performed using one-way ANOVA on parameters that satisfied both
494 conditions (homogeneity and normality of distribution) and using the Kruskal-Wallis test for those that
495 did not. Results are presented as means +/-SEM. Significance level was set at $p \leq 0.05$.

496 **Acknowledgments**

497 This project was funded by a springboard fellowship from Target ALS to KAQ and a University of Rhode
498 Island Graduate School Tuition Scholarship to LMM. The authors made use of equipment supported by

499 the Institutional Development Award (IDeA) Network for Biomedical Research Excellence from the
500 National Institute of General Medical Sciences of the National Institutes of Health under grant number
501 P20GM103430. The authors thank Drs Emily Reedich, Claudia Fallini and Marin Manuel for comments on
502 the initial drafts of the manuscript.
503

504 **References**

505 Akay T (2014) Long-term measurement of muscle denervation and locomotor behavior in individual
506 wild-type and ALS model mice. J Neurophysiol 111:694–703.
507 Allain A-E, Bairi A, Meyrand P, Branchereau P (2006) Expression of the Glycinergic System During the
508 Course of Embryonic Development in the Mouse Spinal Cord and its Co-Localization with GABA
509 Immunoreactivity. J Comp Neurol 496:832–846.
510 Allodi I, Montañana-Rosell R, Selvan R, Löw P, Kiehn O (2021) Locomotor deficits in a mouse model of
511 ALS are paralleled by loss of V1-interneuron connections onto fast motor neurons. Nat Commun 12:1–
512 18 Available at: http://dx.doi.org/10.1038/s41467-021-23224-7.
513 Amendola J, Durand J (2008) Morphological differences between wild-type and transgenic superoxide
514 dismutase 1 lumbar motoneurons in postnatal mice. J Comp Neurol 511:329–341.
515 Andreadou E, Kapaki E, Kokotis P, Paraskevas GP, Katsaros N, Libitaki G, Petropoulou O, Zis V, Sfagos C,
516 Vassilopoulos D (2008) Plasma glutamate and glycine levels in patients with amyotrophic lateral
517 sclerosis. In Vivo (Brooklyn) 22:137–142.
518 Avossa D, Grandolfo M, Mazzarol F, Zatta M, Ballerini L (2006) Early signs of motoneuron vulnerability in
519 a disease model system: Characterization of transverse slice cultures of spinal cord isolated from
520 embryonic ALS mice. Neuroscience 138:1179–1194.
521 Bae JS, Simon NG, Menon P, Vucic S, Kiernan C, Doyle AC, Case-book T, Holmes S (2013) The Puzzling
522 Case of Hyperexcitability in Amyotrophic Lateral Sclerosis What Really is Hyperexcitability in ALS ? How
523 Can We Objectively Assess. J Clin Neurol 9:65–74.
524 Bensimon G, Lacomblez L, Meininger V (1994) A Controlled Trial of Riluzole in Amyotrophic Lateral
525 Sclerosis. N Engl J Med 330:585–591.
526 Bikoff JB, Gabitto MI, Rivard AF, Drobac E, Machado TA, Miri A, Brenner-Morton S, Famojure E, Diaz C,
527 Alvarez FJ, Mentis GZ, Jessell TM (2016) Spinal Inhibitory Interneuron Diversity Delineates Variant Motor
528 Microcircuits. Cell 165:207–219 Available at:
529 http://www.embase.com/search/results?subaction=viewrecord&from=export&id=L608793625%0Ahttp:
530 //dx.doi.org/10.1016/j.cell.2016.01.027.
531 Branchereau P, Martin E, Supiot L, Hodeib F, Laupénie A, Dalvi U, Zhu H, Cazenave W, Cattaert D (2019)
532 Relaxation of synaptic inhibitory events as a compensatory mechanism in fetal SOD spinal motor
533 networks. Elife 8:1–28.
534 Casas C, Herrando-Grabulosa M, Manzano R, Mancuso R, Osta R, Navarro X (2013) Early presymptomatic

535 cholinergic dysfunction in a murine model of amyotrophic lateral sclerosis. Brain Behav 3:145–158.
536 Chang Q, Martin LJ (2009a) Glycinergic Innervation of Motoneurons Is Deficient in Amyotrophic Lateral
537 Sclerosis Mice A Quantitative Confocal Analysis. Am J Pathol 174:574–585.
538 Chang Q, Martin LJ (2009b) Glycinergic innervation of motoneurons is deficient in amyotrophic lateral
539 sclerosis mice: A quantitative confocal analysis. Am J Pathol 174:574–585.
540 Clark RM, Blizzard CA, Young KM, King AE, Dickson TC (2017) Calretinin and Neuropeptide y interneurons
541 are differentially altered in the motor cortex of the SOD1 G93A mouse model of ALS. Sci Rep 7:1–13
542 Available at: http://dx.doi.org/10.1038/srep44461.
543 Clark RM, Brizuela M, Blizzard CA, Dickson TC (2018) Reduced excitability and increased neurite
544 complexity of cortical interneurons in a familial mouse model of amyotrophic lateral sclerosis. Front Cell
545 Neurosci 12:1–7.
546 Delestrée N, Manuel M, Iglesias C, Elbasiouny SM, Heckman CJ, Zytnicki D (2014) Adult spinal
547 motoneurones are not hyperexcitable in a mouse model of inherited amyotrophic lateral sclerosis. J
548 Physiol 592:1687–1703.
549 Devlin AC, Burr K, Borooah S, Foster JD, Cleary EM, Geti I, Vallier L, Shaw CE, Chandran S, Miles GB
550 (2015) Human iPSC-derived motoneurons harbouring TARDBP or C9ORF72 ALS mutations are
551 dysfunctional despite maintaining viability. Nat Commun 6:1–12 Available at:
552 http://dx.doi.org/10.1038/ncomms6999.
553 Dukkipati SS, Chihi A, Wang Y, Elbasiouny SM (2016) Experimental Design and Data Analysis Issues
554 Contribute to Inconsistent Results of C-Bouton Changes in Amyotrophic Lateral Sclerosis. eNeuro 4:1–
555 13.
556 Dukkipati SS, Garrett TL, Elbasiouny SM (2018) The vulnerability of spinal motoneurons and soma size
557 plasticity in a mouse model of amyotrophic lateral sclerosis. J Physiol 596:1723–1745.
558 Filipchuk AA, Durand J (2012) Postnatal dendritic development in lumbar motoneurons in mutant
559 superoxide dismutase 1 mouse model of amyotrophic lateral sclerosis. Neuroscience 209:144–154
560 Available at: http://dx.doi.org/10.1016/j.neuroscience.2012.01.046.
561 Flynn JR, Conn VL, Boyle KA, Hughes DI, Watanabe M, Velasquez T, Goulding MD, Callister RJ, Graham
562 BA (2017) Anatomical and molecular properties of long descending propriospinal neurons in mice. Front
563 Neuroanat 11:1–13.
564 Fogarty MJ, Kanjhan R, Bellingham MC, Noakes PG (2016) Glycinergic neurotransmission: A potent
565 regulator of embryonic motor neuron dendritic morphology and synaptic plasticity. J Neurosci 36:80–87.

566 Genç B, Jara JH, Lagrimas AKB, Pytel P, Roos RP, Mesulam MM, Geula C, Bigio EH, Özdinler PH (2017)
567 Apical dendrite degeneration, a novel cellular pathology for Betz cells in ALS. Sci Rep 7:1–10 Available at:
568 http://dx.doi.org/10.1038/srep41765.
569 Gunes ZI, Kan VWY, Ye XQ, Liebscher S (2020) Exciting Complexity: The Role of Motor Circuit Elements in
570 ALS Pathophysiology. Front Neurosci 14:1–30.
571 Hayashi H, Suga M, Satake M, Tsubaki T (1981) Reduced glycine receptor in the spinal cord in
572 amyotrophic lateral sclerosis. Ann Neurol 9:292–294.
573 Hegedus J, Putman CT, Gordon T (2007) Time course of preferential motor unit loss in the SOD1G93A
574 mouse model of amyotrophic lateral sclerosis. Neurobiol Dis 28:154–164.
575 Herron LR, Miles GB (2012) GENDER-SPECIFIC PERTURBATIONS IN MODULATORY INPUTS TO
576 MOTONEURONS IN A MOUSE MODEL OF AMYOTROPHIC LATERAL SCLEROSIS. Neuroscience 226:313–
577 323 Available at: http://dx.doi.org/10.1016/j.neuroscience.2012.09.031.
578 Hossaini M, Cano SC, Van Dis V, Haasdijk ED, Hoogenraad CC, Holstege JC, Jaarsma D (2011) Spinal
579 inhibitory interneuron pathology follows motor neuron degeneration independent of glial mutant
580 superoxide dismutase 1 expression in SOD1-ALS mice. J Neuropathol Exp Neurol 70:662–677.
581 Howells J, Sangari S, Matamala JM, Kiernan MC, Marchand-Pauvert V, Burke D (2020) Interrogating
582 interneurone function using threshold tracking of the H reflex in healthy subjects and patients with
583 motor neurone disease. Clin Neurophysiol.
584 Irvin CW, Kim RB, Mitchell CS (2015) Seeking homeostasis: Temporal trends in respiration, oxidation, and
585 calcium in SOD1 G93A amyotrophic lateral sclerosis mice. Front Cell Neurosci 9:1–11.
586 Jensen DB, Kadlecova M, Allodi I, Meehan CF (2020) Spinal motoneurones are intrinsically more
587 responsive in the adult G93A SOD1 mouse model of Amyotrophic Lateral Sclerosis. J Physiol.
588 Jonas P, Bischofberger J, Sandkühler J (1998) Corelease of two fast neurotransmitters at a central
589 synapse. Science (80-) 281:419–424.
590 Kim J, Hughes EG, Shetty AS, Arlotta P, Goff LA, Bergles DE, Brown SP (2017) Changes in the Excitability
591 of Neocortical Neurons in a Mouse Model of Amyotrophic Lateral Sclerosis Are Not Specific to
592 Corticospinal Neurons and Are Modulated by Advancing Disease. J Neurosci 37:9037–9053 Available at:
593 http://www.jneurosci.org/lookup/doi/10.1523/JNEUROSCI.0811-17.2017.
594 Kuo JJ, Schonewille M, Siddique T, Schults AN, Fu R, Bar PR, Anelli R, Heckman C, Kroese AB (2004)
595 Hyperexcitability of Cultured Spinal Motoneurons From Presymptomatic ALS Mice. J Neurophysiol
596 91:571–575 Available at: http://jn.physiology.org/cgi/doi/10.1152/jn.00665.2003.

597 Kuo JJ, Siddique T, Fu R, Heckman CJ (2005) Increased persistent Na+ current and its effect on
598 excitability in motoneurones cultured from mutant SOD1 mice. J Physiol 563:843–854.
599 Kuo SW, Binder MD, Heckman CJ (2020) Excessive Homeostatic Gain in Spinal Motoneurons in a Mouse
600 Model of Amyotrophic Lateral Sclerosis. Sci Rep 10.
601 Landoni LM, Myles JR, Wells TL, Mayer WP, Akay T (2019) Cholinergic modulation of motor neurons
602 through the C-boutons are necessary for the locomotor compensation for severe motor neuron loss
603 during amyotrophic lateral sclerosis disease progression. Behav Brain Res 369.
604 Leroy F, Lamotte d'Incamps B, Imhoff-Manuel RD, Zytnicki D (2014) Early intrinsic hyperexcitability does
605 not contribute to motoneuron degeneration in amyotrophic lateral sclerosis. Elife 3:1–25.
606 Malessa S, Leigh PN, Bertel O, Sluga E, Hornykiewicz O (1991) Amyotrophic lateral sclerosis: glutamate
607 dehydrogenase and transmitter amino acids in the spinal cord. J Neurol Neurosurg Psychiatry 54:984–
608 988.
609 Martin E, Cazenave W, Cattaert D, Branchereau P (2013) Embryonic alteration of motoneuronal
610 morphology induces hyperexcitability in the mouse model of amyotrophic lateral sclerosis. Neurobiol Dis
611 54:116–126.
612 Martin LJ, Liu Z, Chen K, Price AC, Pan Y, Swaby JA, Golden WC (2007) Motor Neuron Degeneration in
613 Amyotrophic Lateral Sclerosis Mutant Superoxide Dismutase-1 Transgenic Mice: Mechanisms of
614 Mitochondriopathy and Cell Death. J Comp Neurol 500:20–46.
615 Martinez-Silva M de L, Imhoff-Manuel RD, Sharma A, Heckman C, Shneider NA, Roselli F, Zytnicki D,
616 Manuel M (2018) Hypoexcitability precedes denervation in the large fast-contracting motor units in two
617 unrelated mouse models of ALS. Elife 7:1–26.
618 McGown A, McDearmid JR, Panagiotaki N, Tong H, Al Mashhadi S, Redhead N, Lyon AN, Beattie CE, Shaw
619 PJ, Ramesh TM (2013) Early interneuron dysfunction in ALS: Insights from a mutant sod1 zebrafish
620 model. Ann Neurol 73:246–258.
621 Medelin M, Rancic V, Cellot G, Laishram J, Veeraraghavan P, Rossi C, Muzio L, Sivilotti L, Ballerini L (2016)
622 Altered development in GABA co-release shapes glycinergic synaptic currents in cultured spinal slices of
623 the SOD1G93Amouse model of amyotrophic lateral sclerosis. J Physiol 594:3827–3840.
624 Milan L, Courtand G, Cardoit L, Masmejean F, Barrière G, Cazalets JR, Garret M, Bertrand SS (2015) Age-
625 related changes in pre- and postsynaptic partners of the cholinergic C-boutons in wild-type and
626 SOD1G93Alumbar motoneurons. PLoS One 10:1–21.
627 Niebroj-Dobosz I, Janik P (1999) Amino acids acting as transmitters in amyotrophic lateral sclerosis (ALS).

Acta Neurol Scand 100:6–11.

Nishimaru H, Sakagami H, Kakizaki M, Yanagawa Y (2011) Locomotor-related activity of GABAergic interneurons localized in the ventrolateral region in the isolated spinal cord of neonatal mice. J Neurophysiol 106:1782–1792.

Ozdinler PH, Benn S, Yamamoto TH, Guzel M, Brown RH, Macklis JD (2011) Corticospinal Motor Neurons and Related Subcerebral Projection Neurons Undergo Early and Specific Neurodegeneration in hSOD1G93A Transgenic ALS Mice. J Neurosci 31:4166–4177 Available at: http://www.jneurosci.org/cgi/doi/10.1523/JNEUROSCI.4184-10.2011.

Özyurt MG, Topkara B, İşak B, Türker KS (2020) Amyotrophic lateral sclerosis weakens spinal recurrent inhibition and post-activation depression. Clin Neurophysiol 131:2875–2886.

Pambo-Pambo A, Durand J, Gueritaud J-P (2009) Early excitability changes in lumbar motoneurons of transgenic SOD1G85R and SOD1G(93A-Low) mice. J Neurophysiol 102:3627–3642 Available at: http://www.ncbi.nlm.nih.gov/pubmed/19828728.

Perry S, Gezelius H, Larhammar M, Hilscher MM, Lamotte d'Incamps B, Leao KE, Kullander K (2015) Firing properties of Renshaw cells defined by Chrna2 are modulated by hyperpolarizing and small conductance ion currents I<inf>h</inf> and I<inf>SK</inf>. Eur J Neurosci 41:887–898.

Pieri M, Carunchio I, Curcio L, Mercuri NB, Zona C (2009) Increased persistent sodium current determines cortical hyperexcitability in a genetic model of amyotrophic lateral sclerosis. Exp Neurol 215:368–379 Available at: http://dx.doi.org/10.1016/j.expneurol.2008.11.002.

Piotrkiewicz M, Hausmanowa-Petrusewicz I (2011) Motoneuron afterhyperpolarisation duration in amyotrophic lateral sclerosis. J Physiol 589:2745–2754.

Plaitakis A, Constantakakis E (1993) Altered metabolism of excitatory amino acids, N-acetyl-aspartate and N-acetyl-aspartylglutamate in amyotrophic lateral sclerosis. Brain Res Bull 30:381–386.

Pullen AH, Athanasiou D (2009) Increase in presynaptic territory of C-terminals on lumbar motoneurons of G93A SOD1 mice during disease progression. Eur J Neurosci 29:551–561.

Pun S, Santos AF, Saxena S, Xu L, Caroni P (2006) Selective vulnerability and pruning of phasic motoneuron axons in motoneuron disease alleviated by CNTF. Nat Neurosci 9:408–419.

Quinlan KA, Kajtaz E, Ciolino JD, Imhoff-Manuel RD, Tresch MC, Heckman CJ, Tysseling VM (2017) Chronic electromyograms in treadmill running SOD1 mice reveal early changes in muscle activation. J Physiol 595:5387–5400.

Quinlan KA, Lamano JB, Samuels J, Heckman CJ (2015) Comparison of dendritic calcium transients in

659 juvenile wild type and SOD1G93A mouse lumbar motoneurons. Front Cell Neurosci 9:1–13 Available at:
660 http://journal.frontiersin.org/article/10.3389/fncel.2015.00139/abstract.
661 Quinlan KA, Schuster JE, Fu R, Siddique T, Heckman CJ (2011) Altered postnatal maturation of electrical
662 properties in spinal motoneurons in a mouse model of amyotrophic lateral sclerosis. J Physiol 589:2245–
663 2260 Available at: http://doi.wiley.com/10.1113/jphysiol.2010.200659.
664 Raynor EM, Shefner JM (1994) Recurrent inhibition is decreased in patients with amyotrophic lateral
665 sclerosis. Neurology 44:2148–2153.
666 Restrepo CE, Lundfald L, Szabó G, Erdélyi F, Zeilhofer HU, Glover JC, Kiehn O (2009) Transmitter-
667 phenotypes of commissural interneurons in the lumbar spinal cord of newborn mice. J Comp Neurol
668 517:177–192.
669 Rothstein JD, Martin LJ, Kuncl RW (1992) Decreased Glutamate Transport by the Brain and Spinal Cord in
670 Amyotrophic Lateral Sclerosis. N Engl J Med 326:1464–1468.
671 Saba L, Viscomi MT, Caioli S, Pignataro A, Bisicchia E, Pieri M, Molinari M, Ammassari-Teule M, Zona C
672 (2016) Altered Functionality, Morphology, and Vesicular Glutamate Transporter Expression of Cortical
673 Motor Neurons from a Presymptomatic Mouse Model of Amyotrophic Lateral Sclerosis. Cereb Cortex
674 26:1512–1528.
675 Saba L, Viscomi MT, Martini A, Caioli S, Mercuri NB, Guatteo E, Zona C (2019) Modified age-dependent
676 expression of NaV1.6 in an ALS model correlates with motor cortex excitability alterations. Neurobiol Dis
677 130:104532 Available at: https://doi.org/10.1016/j.nbd.2019.104532.
678 Sangari S, Iglesias C, El Mendili MM, Benali H, Pradat PF, Marchand-Pauvert V (2016) Impairment of
679 sensory-motor integration at spinal level in amyotrophic lateral sclerosis. Clin Neurophysiol 127:1968–
680 1977.
681 Saxena S, Roselli F, Singh K, Leptien K, Julien JP, Gros-Louis F, Caroni P (2013) Neuroprotection through
682 Excitability and mTOR Required in ALS Motoneurons to Delay Disease and Extend Survival. Neuron
683 80:80–96 Available at: http://dx.doi.org/10.1016/j.neuron.2013.07.027.
684 Shefner JM, Logigian EL (1998) The mixed nerve silent period in normal subjects and patients with
685 amyotrophic lateral sclerosis. Electromyogr Clin Neurophysiol 38:505–510.
686 Siembab VC, Smith CA, Zagoraiou L, Berrocal MC, Mentis GZ, Alvarez FJ (2010) Target selection of
687 proprioceptive and motor axon synapses on neonatal V1-derived Ia inhibitory interneurons and
688 Renshaw cells. J Comp Neurol 518:4675–4701.
689 Vinsant S, Mansfield C, Jimenez-Moreno R, Moore VDG, Yoshikawa M, Hampton TG, Prevette D, Caress

690 J, Oppenheim RW, Milligan C (2013a) Characterization of early pathogenesis in the SOD1G93A mouse
691 model of ALS: Part II, results and discussion. Brain Behav 3:431–457.
692 Vinsant S, Mansfield C, Jimenez-Moreno R, Moore VDG, Yoshikawa M, Hampton TG, Prevette D, Caress
693 J, Oppenheim RW, Milligan C (2013b) Characterization of early pathogenesis in the SOD1G93A mouse
694 model of ALS: Part I, background and methods. Brain Behav 3:335–350.
695 Wainger BJ, Kiskinis E, Mellin C, Wiskow O, Han SSW, Sandoe J, Perez NP, Williams LA, Lee S, Boulting G,
696 Berry JD, Brown RH, Cudkowicz ME, Bean BP, Eggan K, Woolf CJ (2014) Intrinsic membrane
697 hyperexcitability of amyotrophic lateral sclerosis patient-derived motor neurons. Cell Rep 7:1–11
698 Available at: http://dx.doi.org/10.1016/j.celrep.2014.03.019.
699 Whitehouse PJ, Wamsley JK, Zarbin MA, Price DL, Tourtellotte WW, Kuhar MJ (1983) Amyotrophic
700 lateral sclerosis: Alterations in neurotransmitter receptors. Ann Neurol 14:8–16.
701 Willis W, Willis JC (1964) Location of Renshaw Cells. Nature 204:1214–1215.
702 Wootz H, Fitzsimons-Kantamneni E, Larhammar M, Rotterman TM, Enjin A, Patra K, André E, Van
703 Zundert B, Kullander K, Alvarez FJ (2013) Alterations in the motor neuron-renshaw cell circuit in the
704 Sod1G93Amouse model. J Comp Neurol 521:1449–1469.
705 Zeilhofer HU, Studler B, Arabadzisz D, Schweizer C, Ahmadi S, Layh B, Bösl MR, Fritschy JM (2005)
706 Glycinergic neurons expressing enhanced green fluorescent protein in bacterial artificial chromosome
707 transgenic mice. J Comp Neurol 482:123–141.
708
709